Electronic Supplementary Information

Fabrication of core-shell Prussian blue analogues@$ZnIn_2S_4$ nanocubes for efficient photocatalytic hydrogen evolution coupling with biomass furfuryl alcohol oxidation

Yi-Fei Huang[a], Jia-Jia Zhang [a], Ye-Jun Wang [a], Yuan-Sheng Cheng [b], Min Ling [c], Pan Pan [c], Dongdong Liu [a,c], Fang-Hui Wu [a] and Xian-Wen Wei [a,*]

a School of Chemistry and Chemical Engineering, Institute of Materials Sciences and Engineering, Institute of Clean Energy and Advanced Nanocatalysis (iClean), Anhui Province Key Laboratory of Coal Clean Conversion and High Valued Utilization, Anhui University of Technology, Maanshan 243002, China

b School of Metallurgical Engineering, Anhui University of Technology, Maanshan 243002, China

c Anhui Province Key Laboratory of Conservation and Utilization for Dabie Mountain Special Bio-Resources, West Anhui University, Lu'an, 237012, China

1. Experimental

1.1 Materials

$M^{II}(CH_3COO)_2 \cdot nH_2O$ and trisodium citrate were purchased from Adamas. Potassium hexacyanocobaltate and potassium ferricyanide were obtained from Sigma-Aldrich. Other chemicals were of analytical grade and were used without additional purification. Ultrapure water (18.2 MΩ cm) supplied by a Milli-Q system was used throughout the study.

1.2 Photocatalytic performance testing

The photocatalyst performance evaluation was conducted using a multi-channel photochemical reaction system (PCX-50C, Beijing Perfectlight) with a white LED as the light source. The output power of the light source was precisely controlled using an irradiance meter (FZ-A) to maintain a constant irradiance intensity of 100 mW/cm^2. Typically, 12 mL of suspension containing 10 mM furfuryl alcohol and 6 mg of photocatalyst was added to a sealed quartz vessel equipped with a rubber plug and magnetic stirring. The entire system was purged with Ar gas and maintained at 25 °C by a continuous flow of cooling water during the illumination. The gas products were detected using gas chromatography (GC, Agilent 7820A).

1.3 Liquid products analysis

The products for photo-hydrogenation of furfural alcohols (FOL) were analyzed by high-performance liquid chromatography (HPLC, Shimadzu LC-20A). 1 mL of the reaction mixture was filtered by a 0.22 μm filter membrane to remove solid catalyst. HPLC was carried out on a Shimadzu C18 column (150×4.6 mm) with CH_3CN: H_2O

aqueous solution (40:60) as the mobile phase. The flow rate was 0.5 mL/min and the detection wavelength of ultraviolet-visible detector was 230 nm, respectively.

The conversion of FOL and the selectivity of furfural (FAL) were defined as follows:

$$\text{Conversion (\%)} = [(C_0 - C_{FOL})/C_0] \times 100\%,$$

$$\text{Selectivity (\%)} = [C_{FAL}/(C_0 - C_{FOL})] \times 100\%,$$

where C_0 is the initial concentration of FOL, C_{FOL} and C_{FAL} are the concentrations of the substrate FOL and FAL.

1.4 Electrochemical measurements

All the electrochemical measurements were conducted on a three electrode system at an electrochemical station (CHI 660E). The catalyst coated glass carbon electrode or FTO glass were used as the working electrode, Pt as the counter-electrode, and Ag/AgCl or saturated calomel electrode (SCE) as the reference electrode. Linear sweep voltammetry (LSV) was measured at a scan rate of 5 mV s^{-1} to obtain the polarization curves with 0.5 M K_2SO_4 using as electrolyte. Electrochemical impedance spectra (EIS) was recorded at an open circuit voltage in 5 mM $K_3[Fe(CN)_6]$ and $K_4[Fe(CN)_6]$ aqueous solution with 0.1 M KCl. Photocurrent response and Mott-Schottky plots (taken at 1 kHz) were tested at 0.5 M Na_2SO_4, and using sample coated FTO glass as working electrode. All the potentials were displayed versus the reversible hydrogen electrode (RHE) by

$$E_{(RHE)} = E_{(Ag/AgCl)} + 0.197 + 0.059 \times pH$$

1.5 Theoretical calculations

The VASP software[S1,S2] was employed to perform all the spin-polarized density

functional theory (DFT) calculations within the generalized gradient approximation (GGA) using the Perdew-Burke-Ernzerhof (PBE)[S3] formulation. The projected augmented wave (PAW) potentials[S4,S5] were chosen to describe the ionic cores and take valence electrons into account using a plane wave basis set with a kinetic energy cutoff of 400 eV. The Gaussian smearing method and a width of 0.05 eV were utilized to allow partial occupancies of the Kohn−Sham orbitals. The electronic energy was considered self-consistent when the energy change was smaller than 10−6 eV. Convergence of the geometry optimization was determined when the force change was smaller than -0.05 eV/Å2. Grimme's DFT-D3 methodology[S6] was employed to describe the dispersion interactions among all the atoms. A 15 Å vacuum layer in the z direction separated the slab from its periodic images. During structural optimizations of the surface models, a 2×2×1 gamma-point centered k-point grid for the Brillouin zone was used.

2. Supplementary Results

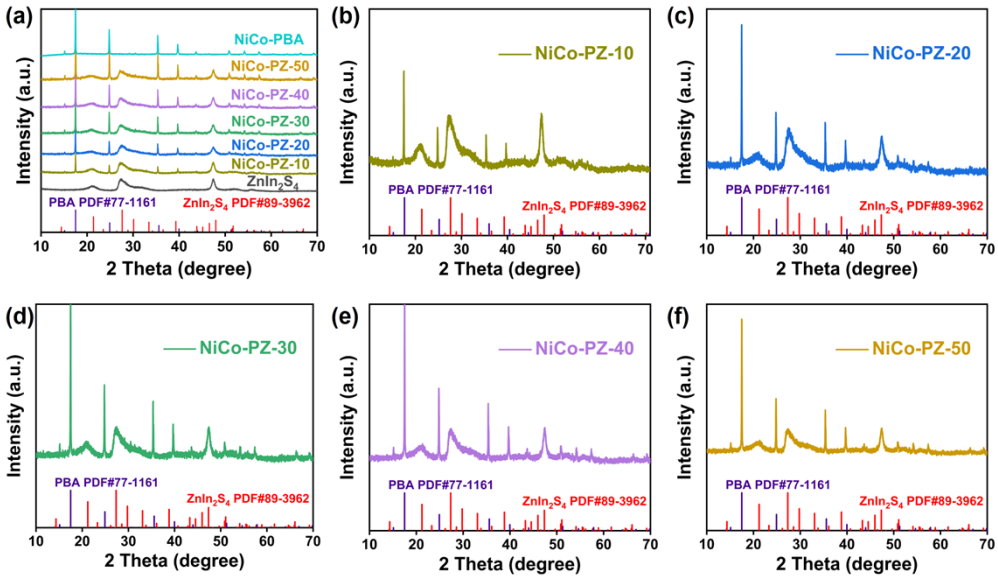

Fig. S1 the XRD patterns of as-prepared samples.

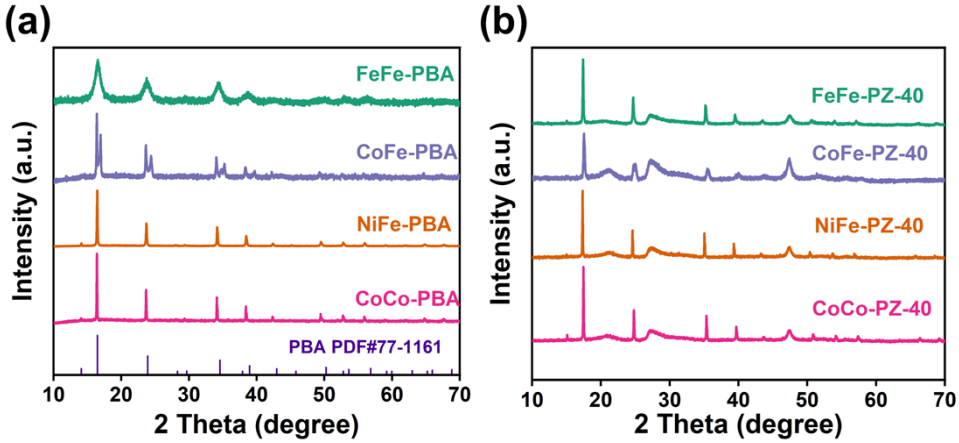

Fig. S2 the XRD patterns of (a) PBA with different metal centers and (b) M^{II}-M^{III} PBA@ZIS with different metal centers.

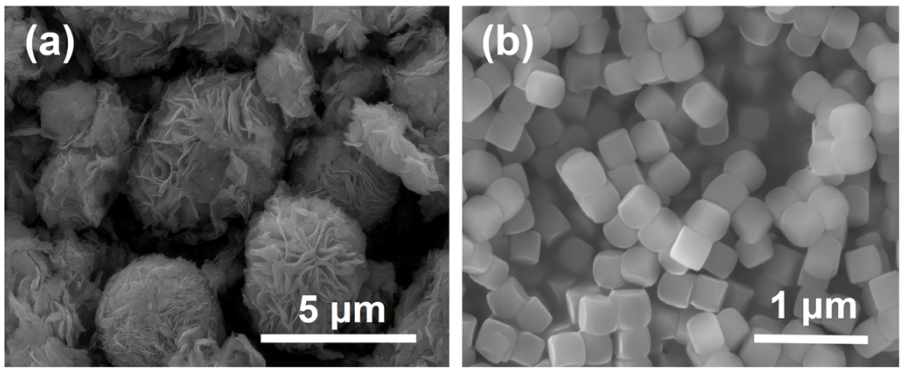

Fig. S3 SEM images of (a) bare $ZnIn_2S_4$ and (b) NiCo-PBA.

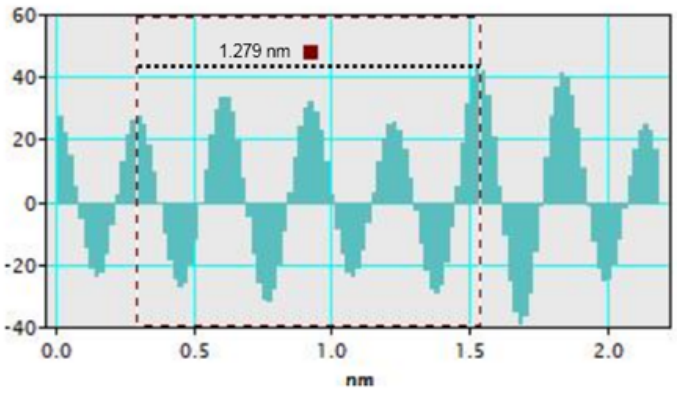

Fig. S4 The result of FFT measurement.

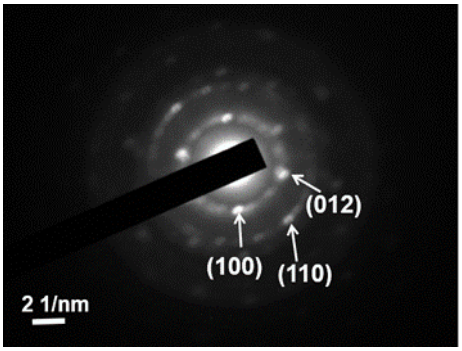

Fig. S5 The selected area electron diffraction (SAED) pattern of NiCo-PZ-40.

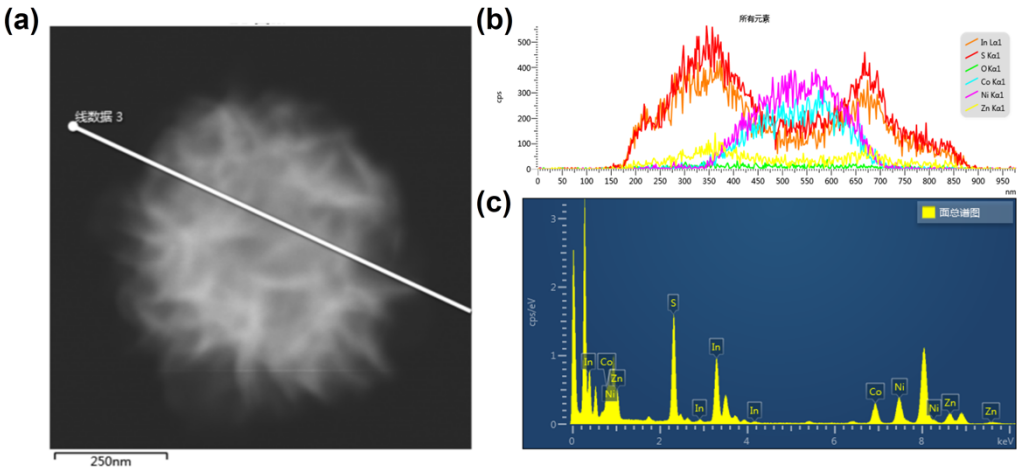

Fig. S6 (a) STEM image, (b) EDX line scanning spectra and (c) raw spectrum of NiCo-PZ-40.

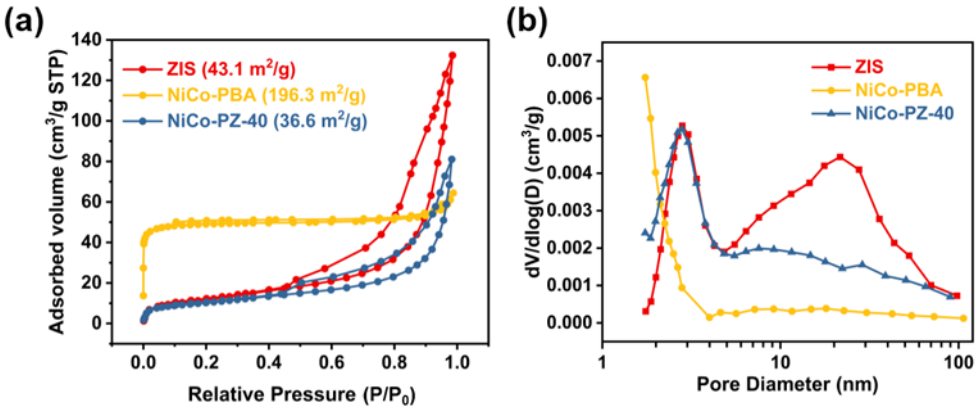

Fig. S7 N_2 adsorption–desorption isotherm curves and pore size distribution of ZIS, NiCo-PBA and NiCo-PZ-40, respectively.

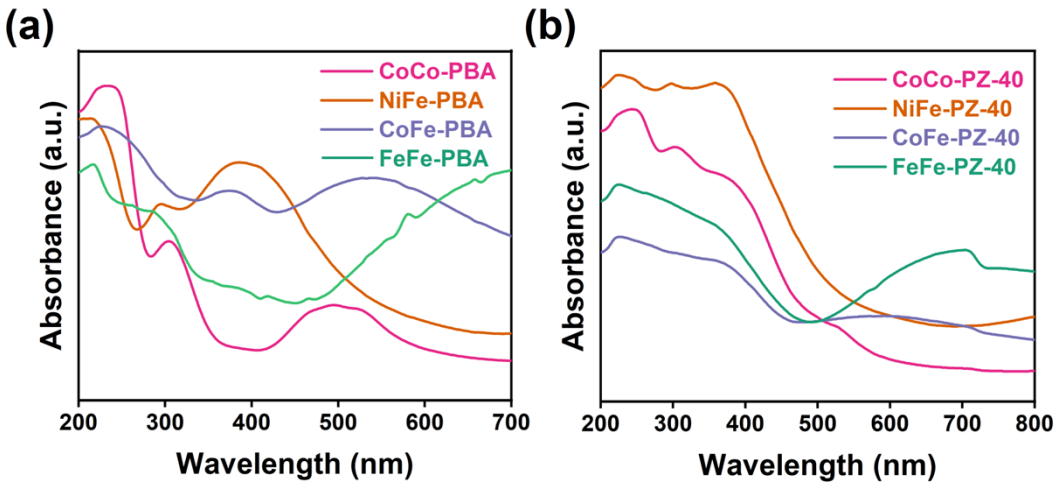

Fig. S8 UV/Vis spectra of (a) PBAs and (b) PBA@ZIS composites with different metals centers.

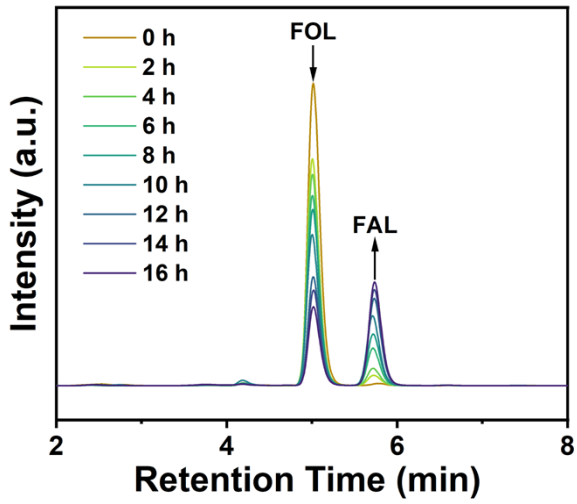

Fig. S9 Time-dependent HPLC chromatograms of the photocatalytic conversion of FOL by NiCo-PZ-40.

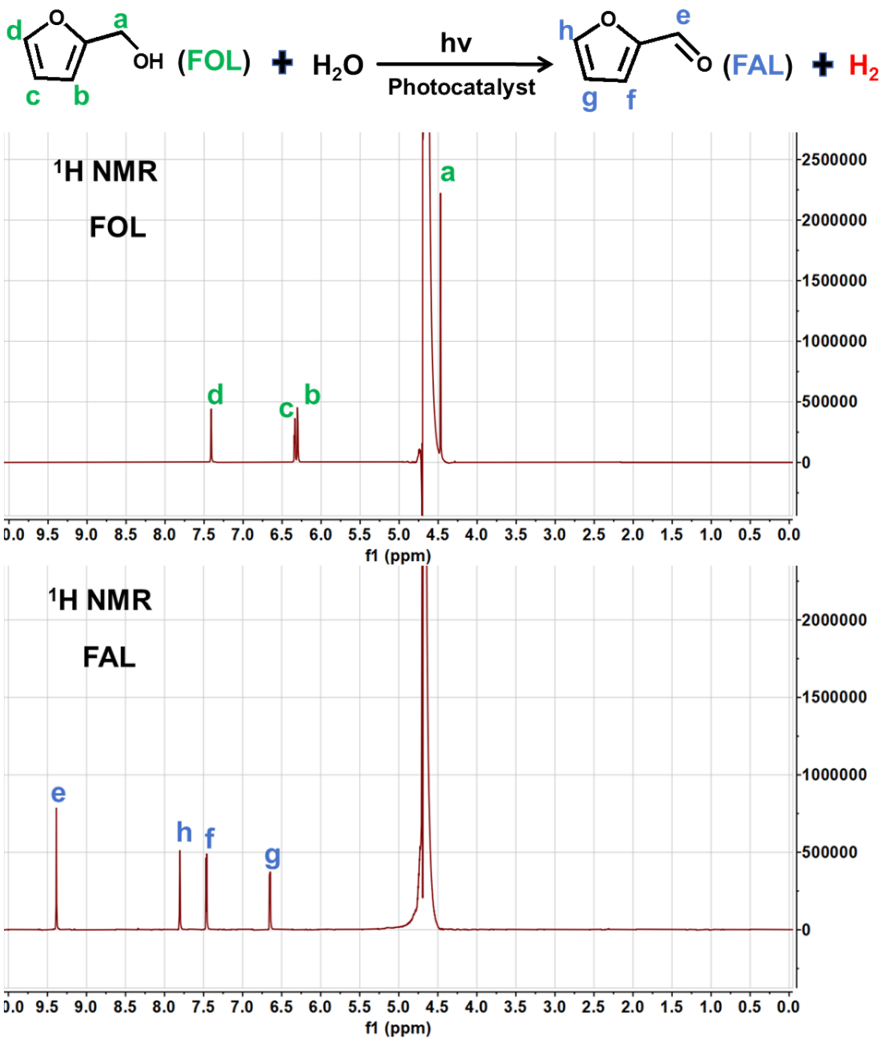

Fig. S10 ^{1}H NMR spectra of standard FOL and FAL.

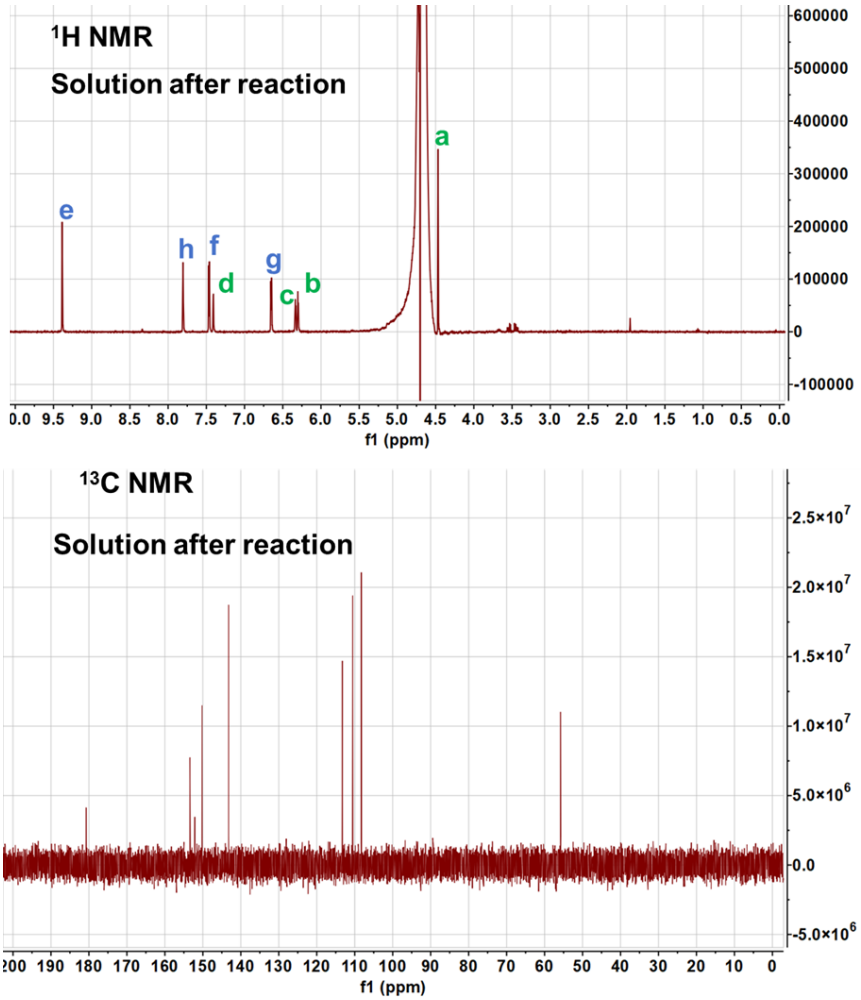

Fig. S11 ^{1}H and ^{13}C NMR spectra of the solution after photocatalytic reaction.

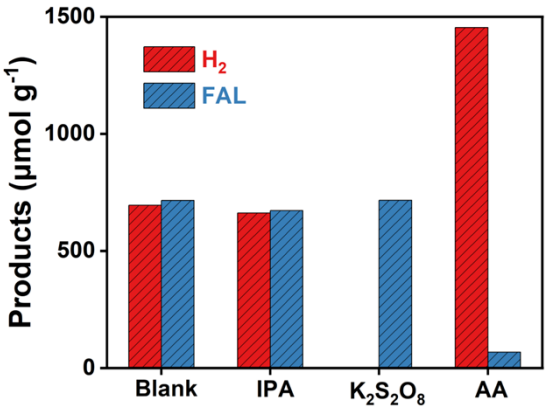

Fig. S12 Control experiments with different additives (20 mM) catalyzed by NiCo-PZ-40 composites photoirradiation for 3 h. (IPA: hydroxyl radicals trapping reagent, $K_2S_2O_8$:electrons trapping reagent and AA: holes trapping reagent).

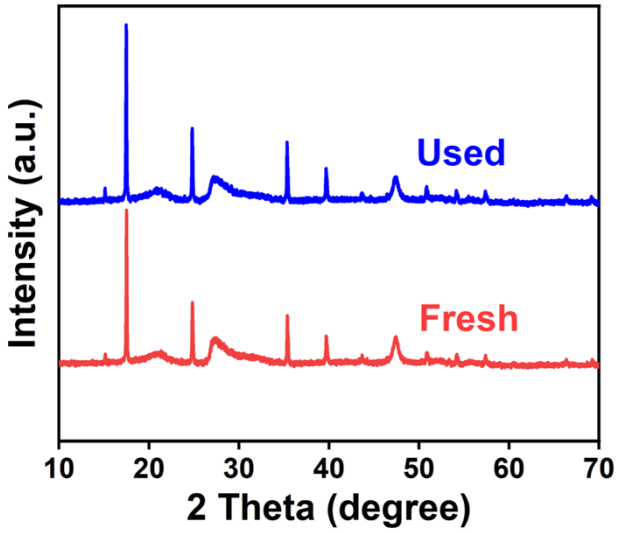

Fig. S13 XRD patterns of NiCo-PZ-40 before and after reaction.

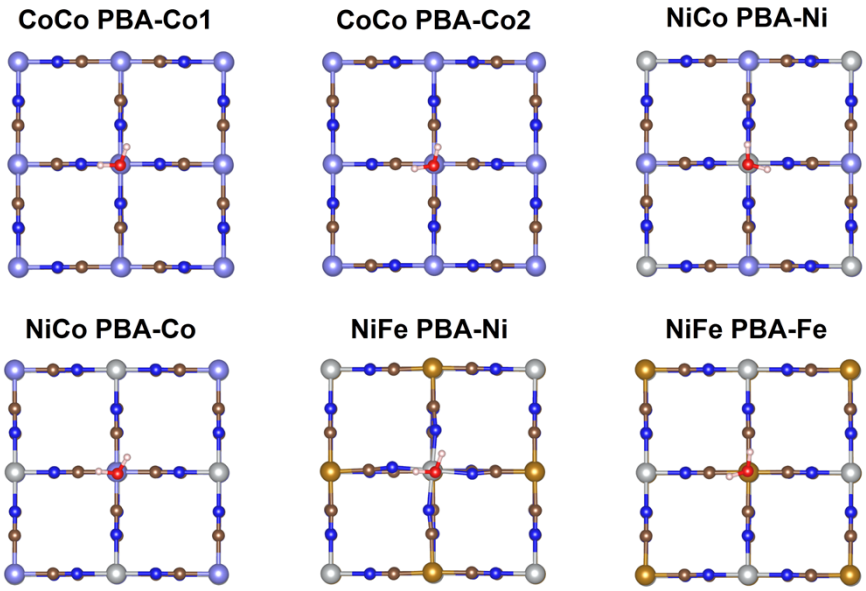

Fig. S14 The DFT calculated models. Light blue, blue, brown, white, red, grey, and bright brown spheres represent Co, N, C, H, O, Ni and Fe atoms, respectively.

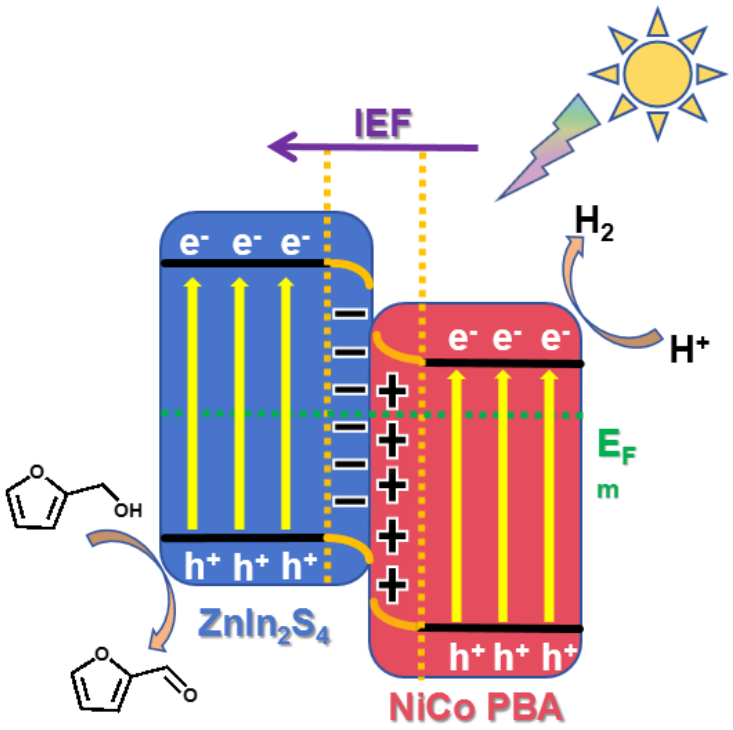

Fig. S15 The photocatalytic coupling mechanism of hydrogen evolution and FAL production.

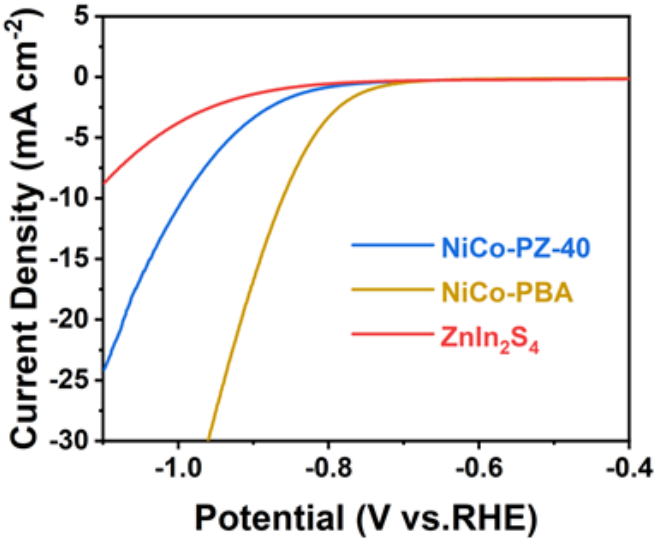

Fig. S16 Linear-sweep voltammograms (LSV) curves of as-prepared samples in 0.5 M K_2SO_4.

Table S1 The metals loading contents in NiCo-PZ-40 estimated by ICP-OES.

Elements	C_0 (mg/L)	C_x (mg/kg)	Weight ratio (%)
Ni	2.9382	109962.6	10.9963%
Co	2.1156	79175.9	7.9176%
Zn	1.6714	62551.2	6.2551%
In	5.9991	224515.7	22.4516%

Table S2 Comparison of recent researches for photocatalytic oxidation of FOL.

Catalyst	Reaction substrate	H_2 evolution ($\mu mol\ g^{-1}\ h^{-1}$)	Liquid yield ($\mu mol\ g^{-1}\ h^{-1}$)	Ref.
NiCo-PZ-40	10 mM FOL	739.3	705.2	This work
$Zn_xIn_2S_{3+x}$	10 mM FOL	584	~	S7
$Ti_3C_2T_x$/CdS	2.5 mM FOL	82	92	S8
3%Pt/$LaVO_4$/CN	10 vol% FOL	287	~	S9
1 wt% Ru/$Zn_{0.5}Cd_{0.5}S$	17 mM FOL	870	855	S10
MCSTC-7.5	50 mM FOL	756.5	764.3	S11
ReS_2/$ZnIn_2S_4$	10 mM FOL	3092.9	2981.1	S12

References

[S1] G. Kresse and J. Furthmüller, Efficiency of Ab-Initio Total Energy Calculations for Metals and Semiconductors Using a Plane-Wave Basis Set, *Comput. Mater. Sci.*, 1996, **6**, 15-50. https://doi.org/10.1016/0927-0256(96)00008-0

[S2] G. Kresse and J. Furthmüller, Efficient Iterative Schemes for Ab Initio Total-Energy Calculations Using a Plane-Wave Basis Set, *Phys. Rev. B*, 1996, **54**, 11169-11186. https://doi.org/10.1103/PhysRevB.54.11169

[S3] J. P. Perdew, K. Burke and M. Ernzerhof, Generalized Gradient Approximation Made Simple, *Phys. Rev. Lett.*, 1996, **77**, 3865-3868. https://doi.org/10.1103/PhysRevLett.77.3865

[S4] G. Kresse and D. Joubert, From Ultrasoft Pseudopotentials to the Projector Augmented-Wave Method, *Phys. Rev. B*, 1999, **59**, 1758-1775. https://doi.org/10.1016/j.commatsci.2019.109237

[S5] P. E. Blöchl, Projector Augmented-Wave Method, *Phys. Rev. B* 1994, **50**, 17953-17979. https://doi.org/10.1103/PhysRevB.50.17953

[S6] S. Grimme, J. Antony, S. Ehrlich and H. Krieg, A consistent and accurate ab initio parametrization of density functional dispersion correction (DFT-D) for the 94 elements H-Pu, *J. Chem. Phys*, 2010, **132**, 15. https://doi.org/10.1063/1.3382344

[S7] D. Gunawan, J. A. Yuwono, P. V. Kumar, A. Kaleem, M. P Nielsen, M. J. Y. Tayebjee, L. O Antwi, H. Wen, I. Kuschnerus, S. L. Y. Chang, Y. Wang, R. K. Hocking, T. S. Chan, C. Y. Toe, J. Scott and R. Amal, Unraveling the structure-activity-selectivity relationships in furfuryl alcohol photoreforming to H_2 and hydrofuroin over $Zn_xIn_2S_{3+x}$ photocatalysts, *Appl. Catal. B Environ.*, 2023, **335**, 122880. https://doi.org/10.1016/j.apcatb.2023.122880.

[S8] Y. H. Li, F. Zhang, Y. Chen, J. Y. Li and Y. J. Xu, Photoredox-catalyzed biomass intermediate conversion integrated with H_2 production over $Ti_3C_2T_x$/CdS composites, *Green Chem.*, 2020, **22**, 163-169. https://doi.org/10.1039/c9gc03332g.

[S9] X. Li, J. Hu, T. Yang, X. Yang, J. Qu and C. M. Li, Efficient photocatalytic H_2-evolution coupled with valuable furfural-production on exquisite 2D/2D $LaVO_4$/g-

C_3N_4 heterostructure, *Nano Energy*, 2022, **92**, 106714.
https://doi.org/10.1016/j.nanoen.2021.106714.

[S10] F. Yang, S. Liu, T. Tang, S. Yao and C. An, Visible-light driven H_2 evolution coupled with furfuryl alcohol selective oxidation over Ru atom decorated $Zn_{0.5}Cd_{0.5}S$ nanorods, *Cataly. Sci. Technol.*, 2023, **13**, 2469-2474.
https://doi.org/10.1039/D2CY01945K.

[S11] S. Zhu, Y. Lin and X. Hong, Cooperative biomass-derived furfural synthesis and H_2 evolution in one photoredox cycle over a $Mn_xCd_{1-x}S/Ti_3C_2$ MXene Schottky junction structure, *Appl. Surf. Sci.*, 2024, **649**, 159139.
https://doi.org/10.1016/j.apsusc.2023.159139.

[S12] Y. S. Cheng, Z. Y. Xing, Zheng X, X. D. Xu, Y. S. Kang, D. Yu, K. L. Wu, F. H. Wu, G. Yuan and X. W. W ei, Integration of ReS_2 on $ZnIn_2S_4$ for boosting the hydrogen evolution coupled with selective oxidation of biomass intermediate under visible light, *Int. J. Hydrogen Energy*, 2023, **48**, 5107-5115. https://doi.org/10.1016/j.ijhydene.2022.11.047.